Critical Role of the Exchange Interaction for the Electronic Structure and Charge-Density-Wave Formation in $TiSe_2$

Maria Hellgren,[1,2] Jacopo Baima,[1] Raffaello Bianco,[3,1] Matteo Calandra,[1] Francesco Mauri,[3,4] and Ludger Wirtz[2]
[1]*Institut de Minéralogie, de Physique des Matériaux et de Cosmochimie, Sorbonne Universités, Université Pierre et Marie Curie, CNRS, IRD, MNHN, 4 Place Jussieu, 75252 Paris, France*
[2]*Physics and Materials Science Research Unit, University of Luxembourg, 162a avenue de la Faïencerie, L-1511 Luxembourg, Luxembourg*
[3]*Dipartimento di Fisica, Università di Roma La Sapienza, Piazzale Aldo Moro 5, I-00185 Roma, Italy*
[4]*Graphene Labs, Fondazione Istituto Italiano di Tecnologia, Via Morego, I-16163 Genova, Italy*
(Received 13 April 2017; revised manuscript received 17 August 2017; published 24 October 2017)

We show that the inclusion of screened exchange via hybrid functionals provides a unified description of the electronic and vibrational properties of $TiSe_2$. In contrast to local approximations in density functional theory, the explicit inclusion of exact, nonlocal exchange captures the effects of the electron-electron interaction needed to both separate the Ti-d states from the Se-p states and stabilize the charge-density-wave (CDW) (or low-T) phase through the formation of a p-d hybridized state. We further show that this leads to an enhanced electron-phonon coupling that can drive the transition even if a small gap opens in the high-T phase. Finally, we demonstrate that the hybrid functionals can generate a CDW phase where the electronic bands, the geometry, and the phonon frequencies are in agreement with experiments.

DOI: 10.1103/PhysRevLett.119.176401

The charge density wave (CDW) instability is a common phenomenon in layered semimetallic transition metal dichalcogenides (TMDs) [1] and has attracted considerable interest over the years, from both the experimental and the theoretical side. The CDW phase is often found to compete with superconductivity and thus plays a similar role as the antiferromagnetic phase in strongly correlated heavy fermion systems or in high-T_c cuprates [2–5]. This intriguing similarity has stimulated the search for a better understanding of the physical mechanism behind the CDW instability in TMDs [6].

The CDW instability in $TiSe_2$ is one of the most studied and debated. On the experimental side, neutron diffraction [7] and x-ray scattering [8] have established the existence of a commensurate $2 \times 2 \times 2$ structural transition at 200 K. This is confirmed by angle resolved photo emission spectroscopy (ARPES) as well as by transport measurements [7], where an abrupt increase in resistivity is found at the same temperature. However, upon further cooling the resistivity reaches an anomalous maximum [7], after which a weak metallic behavior is observed. By contrast, ARPES finds an insulating low-T phase, with a gap of approximately 0.15 eV [9–14]. In the high-T phase ARPES has not been able to conclude whether the system is semimetallic or semiconducting due to the very small indirect (possibly negative) gap. Theoretically, this fact makes $TiSe_2$ an ideal candidate to exhibit an excitonic insulator phase [9,15–17] for which the CDW transition is driven by a purely electronic instability. Some recent experiments [18] partly support this scenario. On the other hand, excitonic correlations alone are insufficient as demonstrated in Ref. [19].

Additional experimental evidence for the CDW instability has been provided by vibrational spectra as a function of temperature. A complete softening of an optical phonon at the L point has been observed in inelastic x-ray scattering experiments [20]. In Raman and infrared (IR) spectroscopy the transition is detected by the appearance of a large number of new modes [21,22], some of which can be related to the CDW transition due to their strong temperature dependence.

On the theoretical side, density functional theory (DFT) within the standard local density approximation (LDA) or the semilocal PBE approximation predicts a structural instability at the correct wave vector [20,23,24] emphasizing the role of the lattice distortion. However, orbital occupations obtained from the electronic band structure are in disagreement with ARPES measurements and CDW phonon frequencies strongly deviate from experiments. This suggests that a proper inclusion of exchange and correlation effects may be crucial to describe the CDW instability. It has been shown that the inclusion of nonlocal exchange already gives a much better description of the electronic bands in both the high- and low-T phase [13,14,25–27]. In Ref. [24] it was further shown that also the DFT + U approach improves the electronic band structure, bringing it into good agreement with ARPES spectra. This seeming improvement, however, was accompanied by a complete loss of the CDW instability.

In this work we provide a unified description of both the electronic band structure and the lattice dynamics of $TiSe_2$, and give a physical explanation for the CDW instability based on first-principles calculations. By an inclusion of

exact exchange within the hybrid functionals we capture the strong Coulomb repulsion due to the localized Ti-d states, thus correcting the orbital occupations. We also capture the long-range exchange interaction which enhances the electron-phonon coupling (EPC) and stabilizes the CDW phase through the formation of a Ti-d-Se-p hybridized state.

$TiSe_2$ is a layered material which in the high-T phase (>200 K) crystallizes in the space group $P\bar{3}m1$. The CDW phase is characterized by a $2 \times 2 \times 2$ superstructure with a different space group $P\bar{3}c1$. The PBE phonon dispersion of the high-T phase was analyzed in Refs. [23] and [24]. The distortion pattern $\mathbf{d}_{3L}$ [see Eq. (9) in Ref. [24]] associated with the imaginary phonon frequencies at the three equivalent L points is of A_u symmetry and its projection on a single $TiSe_2$ layer is shown in the inset of Fig. 1(b). It is completely identified by its symmetry, the magnitude of the displacement δTi and the ratio $\delta\mathrm{Ti}/\delta\mathrm{Se}$. The layers are held together by van der Waals (vdW) forces and in the CDW phase adjacent layers are rotated by 60°. We verified that the vdW forces [28] do not play a role in the CDW distortion and by using the experimentally determined a and c lattice parameters [29] we indirectly account for the vdW contribution to the structure (see also Refs. [24,30]). Although the spin-orbit coupling (SOC) splits the Se-p energy levels [26] it only gives a small contribution to the energetics [30]. Because of the increased computational cost we have, therefore, omitted SOC in the calculations presented here. Local functionals in DFT such as PBE give rise to an excess of electron occupation on the Ti-d states compared to ARPES, mainly due to the large p_z-d band overlap but also due to the overestimated $p_{x,y}$-d band overlap [see black curve in Fig. 1(a)]. To cure this problem it is necessary to include the Coulomb repulsion or "U" due to the localized Ti-d states. A simple corrective procedure to incorporate this effect is the DFT + U approach [31]. Indeed, in Ref. [24] it was shown that the p-d band overlap reduced significantly [see orange curve Fig. 1(a)]. However, it was also found that the energy gain in the distortion decreases by increasing U [30]. The hybrid functionals contain a fraction of exact exchange and, therefore, naturally incorporate the repulsive U interaction [32]. In addition, they exhibit the long-range exchange interaction, which generates the attractive electron-hole interaction at the linear response level [33,34]. The description of screening is rather simplified using a prefactor α and a range-separated Coulomb potential defined by μ. These parameters can be fitted in various ways but often the HSE06 parameters ($\alpha = 0.25$, $\mu = 0.2$ Å^{-1}) give good results [35]. In this work we have used the freedom of varying (α, μ) to reveal the critical role played by exchange, and to shed light on the mechanism that drives the CDW transition in $TiSe_2$.

In Fig. 1(a) we plot the results for the band structure in the high-T phase with PBE, PBE + U, and HSE06 [30,36–40]. In Fig. 1(b) we plot the corresponding energy gain as a function of δTi by displacing the atoms according

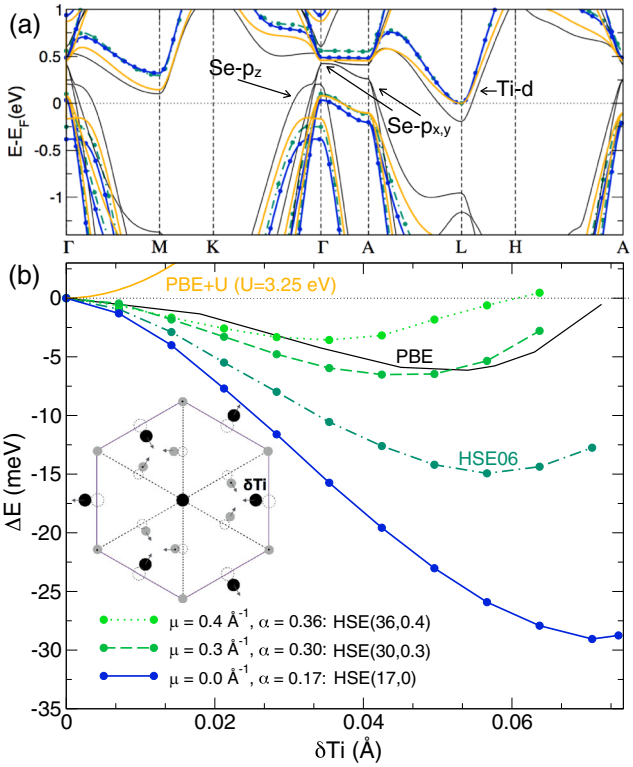

FIG. 1. The upper panel (a) shows the band structure in the high-T phase in PBE (black solid line), HSE06 (green dash-dotted line and circles), HSE(17,0) (blue solid line and circles), and PBE + U ($U = 3.5$ eV) (orange solid line). The lower panel (b) shows the corresponding energy gain as a function of δTi. We show also the results obtained by varying the α and μ parameters such that the band structure around conduction band minimum and valence band maximum is the same as the one of HSE06 and PBE + U.

to the $\mathbf{d}_{3L}$ CDW pattern (using the experimentally determined ratio $\delta\mathrm{Ti}/\delta\mathrm{Se} = 3$ [7]). We found HSE06 to give an enhanced negative curvature and energy gain of approximately a factor of 2 compared to PBE. This difference is mainly attributed to an overscreening at the PBE level, i.e., due to the overestimation of the metallicity of the system. However, this is not the complete picture. We see that PBE + U and HSE06 have almost identical orbital occupations and gaps—both in rather good agreement with experiment [13,14,30]—but in PBE + U the instability is absent. This suggest that the long-range (or nonlocal) Coulomb exchange interaction is important for the formation of the CDW phase, as demonstrated explicitly in Fig. 1(b). We have calculated the energy gain using a set of (α, μ) parameters all tuned to give similar band structures to HSE06 and PBE + U. By reducing the range, i.e., by increasing μ, thus approaching the PBE + U limit, the instability quickly vanishes (green curves). Instead, with an infinite range [HSE(17,0)] the energy gain increases substantially as does the amplitude of the distortion. After relaxing the atomic positions in the CDW phase, we find

δTi = 0.055, 0.061, and 0.082 Å with PBE, HSE06, and HSE(17,0), respectively. In experiment, δTi = 0.085 ± 0.014 Å [7], thus suggesting a long-range (or unscreened) Coulomb interaction. Based on the above analysis, we will continue to discuss the mechanism for the CDW transition, but first we analyze the properties of the CDW phase.

The electronic band structure in comparison with ARPES suggests that the CDW phase is accurately captured with hybrid functionals [14,30]. However, as seen above, a good description of the band structure alone is insufficient. The vibrational frequencies are proportional to the second derivative of the energy and thus provide an additional stringent test for the validity of different approximations. We have calculated the harmonic Raman and IR active phonon frequencies in the CDW phase within both HSE06 and the infinite range HSE(17,0) using a finite difference approach as implemented in the CRYSTAL code [41].

In Fig. 2 we compare the theoretical frequencies with low-T experimental Raman [42] and IR [21] frequencies (at 11 and 20 K, respectively). We analyze the spectra of the CDW phase by backfolding of the phonons at A, L, and M of the high-T phase Brillouin zone [see HSE06 phonon dispersion [43] in Fig. 2(a)] onto the $\bar{\Gamma}$ point of the low-T phase Brillouin zone [30]. In the following, the high-symmetry points of the $2 \times 2 \times 2$ supercell are marked with a bar. For all three approximations, we find an overall good agreement with the experimental results [21,42,44–47]. However, there are three notable exceptions of particular interest for this work: these are the modes related to the instabilities of the high-T structure (marked by vertical dashed lines). The threefold degenerate imaginary phonon frequency at L splits into one A_{1g} and a twofold degenerate E_g mode, which are both Raman active. These have been previously identified as being related to the CDW transition from their experimental temperature dependence [21,22]. In fact, the A_{1g} (amplitude) mode corresponds to the oscillations of the CDW order parameter. The imaginary phonon frequency at M similarly gives rise to an E_u IR active phonon and to one A_{1u} inactive mode. The frequencies of the CDW modes are systematically underestimated by PBE (20% and 30% for the A_{1g} and E_g modes, respectively). HSE06 brings these frequencies in much better agreement with experiment (now underestimated by 4% and 7%, respectively). HSE(17,0), which gave the best geometry, also gives excellent CDW mode frequencies (overestimated by 5% and 2%, respectively). Since the frequencies of these modes depend very sensitively on the CDW potential energy surface [compare Fig. 1(b)], they represent an important confirmation that the hybrid functionals reliably reproduce the electronic structure of $TiSe_2$.

With a reliable description of the vibrational and electronic properties, we can now analyze in detail the physical mechanism that is responsible for the CDW instability in $TiSe_2$. Figure 3(a) shows the HSE06 band structure in both the low-T and high-T phase (the latter one is backfolded into the Brillouin zone that corresponds to the $2 \times 2 \times 2$ supercell of the low-T phase). At the CDW distortion, the threefold degenerate Ti-d band splits into a band with dominant d_{z^2} character derived from the Ti atom in the supercell that does not move with the distortion, and a twofold degenerate band with Ti-d and Se-p hybridization in a small region around $\bar{\Gamma}$ due to the interaction between the p and d states. Similarly, the Se-p bands move to lower energy and hybridize with Ti-d states around $\bar{\Gamma}$. Such p-d hybridization, discussed also in Refs. [11,48,49], is observed by studying the site-projected orbitals onto spherical harmonics before and after the transition. Panel (b) presents a zoom of the region around $\bar{\Gamma}$, showing the effect of a small $\mathbf{d}_{3L}$ distortion on the electronic structure. We see that the distortion only changes the p-d gap while leaving the rest of the electronic structure almost unaffected. We can, therefore, assume that it is

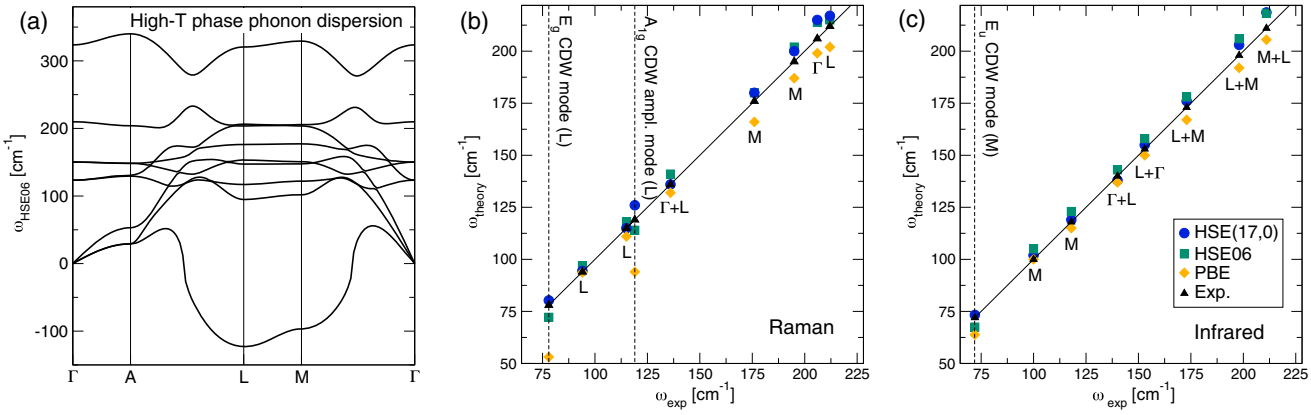

FIG. 2. (a) Phonon dispersion of the high-T phase (HSE06). (b)–(c) Experimental [21,42] versus calculated phonon frequencies of Raman and IR modes in the low-T phase. Modes related to the CDW distortion are marked by vertical dashed lines. The labels refer to the largest components of the phonon eigenvector with respect to the eigenvectors of the high-T structure.

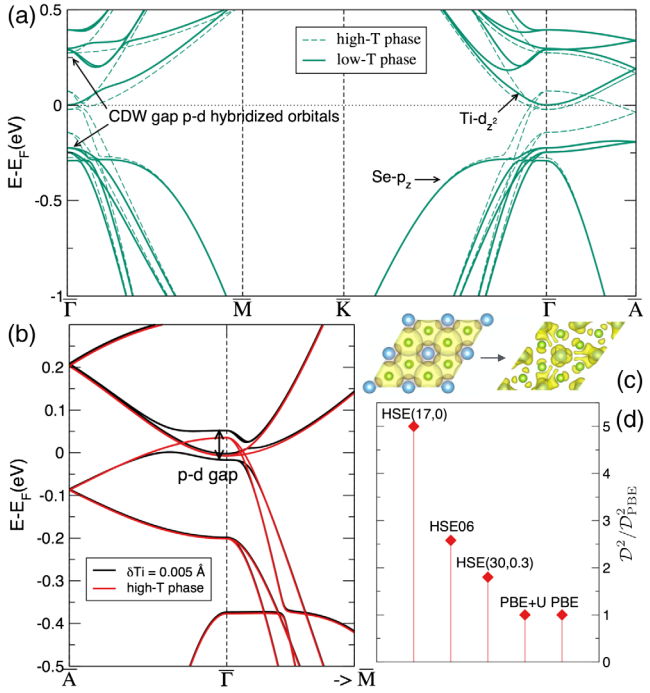

FIG. 3. (a) HSE06 band structure of undistorted (high-T) and CDW (low-T) phases of $TiSe_2$. Panel (b) shows a zoom around the Fermi level and the EPC between the p-d states is calculated in panel (d). The value for $\mathcal{D}^2_{\rm PBE} = 8$ eV^2/Å^2 (where d_{3L} is measured in units of δTi at constant δTi/δSe $= 3$). Panel (c) demonstrates the mixing (hybridization) of these orbitals [57] in the CDW phase.

mainly the p-d states around $\bar{\Gamma}$ which are involved in the transition and extract the EPC, or, more precisely, the deformation potential $\mathcal{D}$ for the different approximations. The deformation potential is defined as $\mathcal{D} = \langle \bar{\Gamma} d | \delta V / \delta d_{3L} | \bar{\Gamma} p \rangle$, where the variation of the total self-consistent potential V is taken with respect to the magnitude d_{3L} of the $\mathbf{d}_{3L}$ distortion. The states $|\bar{\Gamma} d\rangle$ and $|\bar{\Gamma} p\rangle$ with energy difference $\mathcal{E}_0$ are obtained from the Ti-d and Se-p states at L and Γ in the undistorted unit cell by backfolding them onto $\bar{\Gamma}$ in the supercell. Without loss of generality, all quantities can be taken as real in the supercell. The p and d states are superimposed and illustrated in Fig. 3(c) together with the p-d hybridized state in the CDW phase. We also note from first order perturbation theory that $\mathcal{D} = \langle \delta(\bar{\Gamma} d)/\delta d_{3L} | \bar{\Gamma} p \rangle \times \mathcal{E}_0$ and hence (at fixed $\mathcal{E}_0$) $\mathcal{D}$ measures the overlap between the variation of the d state with the distortion and the undistorted p state. We then obtain $\mathcal{D}$ using a finite difference approach [50]. At small but finite d_{3L} we construct the 2×2 submatrix of the Hamiltonian $\mathcal{H}$: $\mathcal{H}_{dd} = -\mathcal{E}_0/2 + \mathcal{O}(d^2_{3L})$, $\mathcal{H}_{pp} = \mathcal{E}_0/2 + \mathcal{O}(d^2_{3L})$ and $\mathcal{H}_{pd} = \mathcal{H}_{dp} = \mathcal{D} d_{3L} + \mathcal{O}(d^2_{3L})$ and diagonalize it to obtain $\mathcal{D}^2 = \frac{1}{4}(\mathcal{E}^2 - \mathcal{E}_0^2)/d^2_{3L}$, where $\mathcal{E}$ is the p-d gap upon the distortion and we have discarded the higher order terms in d_{3L}. The results obtained from this procedure can be found in Fig. 3(d). Although some coupling already exists between p and d states at the PBE level, the deformation potential (and so the EPC) is strongly enhanced via the nonlocal exchange potential in V provided by the inclusion of long-range exchange. Indeed, a comparison between PBE and PBE+U shows that U has no effect on the EPC. For the approximations with the same band structure we see the same trend in Figs. 1(b) and 3(d) and, hence, we conclude that it is the nonlocal exchange interaction that determines the strength of the instability. The inclusion of SOC splits and slightly changes the dispersion of the Se-p bands close to the Fermi level but has only a small quantitative effect on the EPC [30,51]. Our result goes in line with some previous findings that the EPC can be strongly enhanced by nonlocal exchange, notably in weakly doped 2D materials [50,52–54] and some high-T_c superconductors [55]. Although the band structure in HSE06, which we used as a reference, has a small negative p-d gap (−0.1 eV) in the high-T phase, the instability does not crucially depend on the existence of a Fermi surface. In fact, due to the enhanced EPC, the CDW phase can exist even if the gap in the high-T phase is positive. This is easily demonstrated by increasing the amount of exact-exchange (α). With $\mu = 0.2$ Å^{-1} fixed, the instability persists up to $\alpha = 0.35$ when the gap is as large as 0.2 eV. At larger values of the gap (or α) the hybridization of Ti-d and Se-$p_{x,y}$ bands is suppressed and the instability disappears. If we instead decrease $\alpha < 0.25$ the energy gain reaches a maximum around $\alpha = 0.15$. At smaller values of α the CDW phase becomes metallic and the energy gain drops. This unusual behavior as a function of α (or the gap) shares some features with the excitonic insulator transition (EIT) of Kohn *et al.* [15,56]. The EIT arises in a two band model (similar to the p and d bands in $TiSe_2$) when tuned until the value of the p-d gap is smaller than the exciton binding energy. As a result, p and d orbitals mix and form a new ground state with lower symmetry. Since the symmetry of the lattice is kept fixed, the EIT is a purely electronic effect. In our calculations it was not possible to generate a symmetry lowering of the electronic density alone. The mechanism that we found relies on the simultaneous lattice distortion and strong EPC, enhanced by the exchange interaction. Whether the system is still influenced by excitonic effects can be determined by studying the excitation spectrum, but this we leave for future work.

M. H. and L. W. gratefully acknowledge financial support from the FNR (projects RPA-phonon and INTER/ANR/13/20/NANOTMD). The authors acknowledge support from the European Union Horizon 2020 research and innovation programme under Grant agreement No. 696656-GrapheneCore1 and by Agence Nationale de la Recherche under the reference No. ANR-13-IS10-0003-01 and by Prace. Calculations were performed at IDRIS, CINES, CEA, and BSC TGCC. The authors are grateful to K. Rossnagel for having supplied to them the image data of the ARPES experiment.

[1] J. A. Wilson, F. J. D. Salvo, and S. Mahajan, Adv. Phys. **24**, 117 (1975).
[2] S. Y. Li, G. Wu, X. H. Chen, and L. Taillefer, Phys. Rev. Lett. **99**, 107001 (2007).
[3] A. F. Kusmartseva, B. Sipos, H. Berger, L. Forró, and E. Tutiš, Phys. Rev. Lett. **103**, 236401 (2009).
[4] E. Morosan, H. W. Zandbergen, B. S. Dennis, J. W. G. Bos, Y. Onose, T. Klimczuk, A. P. Ramirez, N. P. Ong, and R. J. Cava, Nat. Phys. **2**, 544 (2006).
[5] D. Qian, D. Hsieh, L. Wray, E. Morosan, N. L. Wang, Y. Xia, R. J. Cava, and M. Z. Hasan, Phys. Rev. Lett. **98**, 117007 (2007).
[6] K. Rossnagel, J. Phys. Condens. Matter **23**, 213001 (2011).
[7] F. J. Di Salvo, D. E. Moncton, and J. V. Waszczak, Phys. Rev. B **14**, 4321 (1976).
[8] Y. I. Joe, X. M. Chen, P. Ghaemi, K. D. Finkelstein, G. A. de la Pena, Y. Gan, J. C. T. Lee, S. Yuan, J. Geck, G. J. MacDougall, T. C. Chiang, S. L. Cooper, E. Fradkin, and P. Abbamonte, Nat. Phys. **10**, 421 (2014).
[9] T. Pillo, J. Hayoz, H. Berger, F. Lévy, L. Schlapbach, and P. Aebi, Phys. Rev. B **61**, 16213 (2000).
[10] T. E. Kidd, T. Miller, M. Y. Chou, and T.-C. Chiang, Phys. Rev. Lett. **88**, 226402 (2002).
[11] K. Rossnagel, L. Kipp, and M. Skibowski, Phys. Rev. B **65**, 235101 (2002).
[12] H. Cercellier, C. Monney, F. Clerc, C. Battaglia, L. Despont, M. G. Garnier, H. Beck, P. Aebi, L. Patthey, H. Berger, and L. Forró, Phys. Rev. Lett. **99**, 146403 (2007).
[13] P. Chen, Y. H. Chan, X. Y. Fang, Y. Zhang, M. Y. Chou, S. K. Mo, Z. Hussain, A. V. Fedorov, and T. C. Chiang, Nat. Commun. **6**, 8943 (2015).
[14] Y.-H. P. Chen, X. Chan, S. Fang, Z. Mo, Z. Hussain, A. V. Fedorov, M. Chou, and T. C. Chiang, Sci. Rep. **6**, 37910 (2016).
[15] D. Jérome, T. M. Rice, and W. Kohn, Phys. Rev. **158**, 462 (1967).
[16] C. Monney, H. Cercellier, F. Clerc, C. Battaglia, E. F. Schwier, C. Didiot, M. G. Garnier, H. Beck, P. Aebi, H. Berger, L. Forró, and L. Patthey, Phys. Rev. B **79**, 045116 (2009).
[17] C. Monney, C. Battaglia, H. Cercellier, P. Aebi, and H. Beck, Phys. Rev. Lett. **106**, 106404 (2011).
[18] T. Rohwer, S. Hellmann, M. Wiesenmayer, C. Sohrt, A. Stange, B. Slomski, A. Carr, Y. Liu, L. M. Avila, M. Kallane, S. Mathias, L. Kipp, K. Rossnagel, and M. Bauer, Nature (London) **471**, 490 (2011).
[19] M. Porer, U. Leierseder, J. M. Ménard, H. Dachraoui, L. Mouchliadis, I. E. Perakis, U. Heinzmann, J. Demsar, K. Rossnagel, and R. Huber, Nat. Mater. **13**, 857 (2014).
[20] F. Weber, S. Rosenkranz, J.-P. Castellan, R. Osborn, G. Karapetrov, R. Hott, R. Heid, K.-P. Bohnen, and A. Alatas, Phys. Rev. Lett. **107**, 266401 (2011).
[21] J. A. Holy, K. C. Woo, M. V. Klein, and F. C. Brown, Phys. Rev. B **16**, 3628 (1977).
[22] C. S. Snow, J. F. Karpus, S. L. Cooper, T. E. Kidd, and T.-C. Chiang, Phys. Rev. Lett. **91**, 136402 (2003).
[23] M. Calandra and F. Mauri, Phys. Rev. Lett. **106**, 196406 (2011).
[24] R. Bianco, M. Calandra, and F. Mauri, Phys. Rev. B **92**, 094107 (2015).
[25] M. Cazzaniga, H. Cercellier, M. Holzmann, C. Monney, P. Aebi, G. Onida, and V. Olevano, Phys. Rev. B **85**, 195111 (2012).
[26] Z. Vydrova, E. F. Schwier, G. Monney, T. Jaouen, E. Razzoli, C. Monney, B. Hildebrand, C. Didiot, H. Berger, T. Schmitt, V. N. Strocov, F. Vanini, and P. Aebi, Phys. Rev. B **91**, 235129 (2015).
[27] Z. Zhu, Y. Cheng, and U. Schwingenschlögl, Phys. Rev. B **85**, 245133 (2012).
[28] S. Grimme, J. Comput. Chem. **27**, 1787 (2006).
[29] C. Riekel, J. Solid State Chem. **17**, 389 (1976).
[30] See Supplemental Material at http://link.aps.org/supplemental/10.1103/PhysRevLett.119.176401 for further information on the computational procedures, crystal structure, spin-orbit coupling, phonon-frequencies, band structures compared to ARPES and the PBE + U approach.
[31] V. I. Anisimov, J. Zaanen, and O. K. Andersen, Phys. Rev. B **44**, 943 (1991).
[32] B. Himmetoglu, A. Floris, S. de Gironcoli, and M. Cococcioni, Int. J. Quantum Chem. **114**, 14 (2014).
[33] J. Paier, M. Marsman, and G. Kresse, Phys. Rev. B **78**, 121201 (2008).
[34] A.-M. Ferrari, R. Orlando, and M. Rerat, J. Chem. Theory Comput. **11**, 3245 (2015).
[35] J. Heyd, G. E. Scuseria, and M. Ernzerhof, J. Chem. Phys. **118**, 8207 (2003).
[36] P. Giannozzi *et al.*, J. Phys. Condens. Matter **21**, 395502 (2009).
[37] R. Dovesi, R. Orlando, A. Erba, C. M. Zicovich-Wilson, B. Civalleri, S. Casassa, L. Maschio, M. Ferrabone, M. D. L. Pierre, P. Darco, Y. Noel, M. Causa, M. Rerat, and B. Kirtman, Int. J. Quantum Chem. **114**, 1287 (2014).
[38] G. Kresse and J. Furthmüller, Phys. Rev. B **54**, 11169 (1996).
[39] G. Kresse and J. Furthmüller, Comput. Mater. Sci. **6**, 15 (1996).
[40] G. Kresse and D. Joubert, Phys. Rev. B **59**, 1758 (1999).
[41] F. Pascale, C. Zicovich-Wilson, F. Lopez, B. Civalleri, R. Orlando, and R. Dovesi, J. Comput. Chem. **25**, 888 (2004).
[42] S. Sugai, K. Murase, S. Uchida, and S. Tanaka, Solid State Commun. **35**, 433 (1980).
[43] The phonon dispersion is approximated on a $2 \times 2 \times 2$ q grid.
[44] S. Uchida and S. Sugai, Physica (Amsterdam) **105**, 393 (1981).
[45] W. Y. Liang, G. Lucovsky, J. C. Mikkelsen, and R. H. Friend, Philos. Mag. Part B **39**, 133 (1979).
[46] J. A. Wilson, Phys. Status Solidi B **86**, 11 (1978).
[47] D. L. Duong, G. Ryu, A. Hoyer, C. Lin, M. Burghard, and K. Kern, ACS Nano **11**, 1034 (2017).
[48] N. G. Stoffel, S. D. Kevan, and N. V. Smith, Phys. Rev. B **31**, 8049 (1985).
[49] J. van Wezel, P. Nahai-Williamson, and S. S. Saxena, Phys. Rev. B **81**, 165109 (2010).
[50] M. Lazzeri, C. Attaccalite, L. Wirtz, and F. Mauri, Phys. Rev. B **78**, 081406 (2008).
[51] M. J. Verstraete, M. Torrent, F. Jollet, G. Zérah, and X. Gonze, Phys. Rev. B **78**, 045119 (2008).

[52] C. Attaccalite, L. Wirtz, M. Lazzeri, F. Mauri, and A. Rubio, Nano Lett. **10**, 1172 (2010).
[53] M. Calandra, P. Zoccante, and F. Mauri, Phys. Rev. Lett. **114**, 077001 (2015).
[54] B. Pamuk, J. Baima, R. Dovesi, M. Calandra, and F. Mauri, Phys. Rev. B **94**, 035101 (2016).
[55] Z. P. Yin, A. Kutepov, and G. Kotliar, Phys. Rev. X **3**, 021011 (2013).
[56] W. Kohn, Phys. Rev. Lett. **19**, 439 (1967).
[57] The iso-surface of the absolute square of the Bloch orbitals were obtained within HSE06 using VASP and VESTA, K. Momma and F. Izumi, J. Appl. Crystallogr. **44**, 1272 (2011).